Phase matching in monolithic Bragg reflection waveguides

A. S. Helmy,* B. Bijlani, and P. Abolghasem

Department of Electrical and Computer Engineering and Institute for Optical Sciences, University of Toronto, 10 King's College Road, Toronto, Ontario M5S 3G4, Canada
**Corresponding author: a.helmy@utoronto.ca*

Received May 29, 2007; accepted June 14, 2007;
posted July 12, 2007 (Doc. ID 83563); published August 6, 2007

We report what is believed to be the first observation of second-harmonic generation by type I phase matching the bulk $\chi^{(2)}_{xyz}$ (d_{14}) nonlinear coefficient using Bragg reflection waveguides. Second-harmonic power of 0.7 μW was observed for a pump wavelength of 1587.8 nm with an average power of 25.2 mW and a pulse width of ~2 ps at a repetition rate of 75.6 MHz. An order of magnitude enhancement between the phase-matched and un-phase-matched second-harmonic conversion efficiency has been observed. Conversion efficiency at the phase-matched wavelengths was 0.001%. The bandwidth of the second harmonic was found to be equal to 0.43 nm, agreeing with the theoretical predictions.

OCIS codes: 190.5970, 160.4330, 130.3120, 230.7370, 230.1480, 190.2620.

Photonic and optoelectronic devices based on the second-order nonlinear coefficient $\chi^{(2)}$ can offer distinct advantages over their conventional counterparts. Harnessing efficient second-order nonlinearities in compound semiconductors can enable devices such as electrically pumped monolithic optical parametric oscillators (OPOs), parametric optical amplifiers, correlated photon pair sources, difference frequency generation elements with integrated tuning sources, and all-optical signal processing elements. There are advantages offered by compound semiconductors in comparison with conventional bulk nonlinear crystals and periodically poled lithium niobate structures. These include the inherently large nonlinearities they exhibit, a wide transparency window extending between 1 and 18 μm, mature fabrication technology, as well as the ability to integrate active and passive devices.

Associated with their large nonlinearities, semiconductors also possess large dispersion. Both take place at wavelengths close to their bandgap. This renders the problems of phase matching in such material systems challenging. For second-harmonic generation (SHG) using $\chi^{(2)}$ nonlinearities, the effective indices of both waves need to be equal for phase matching to take place, namely $n_{2\omega}=n_{\omega}$. The difficulty of achieving this in semiconductors is usually most severe while operating near the bandgap resonances where dispersion prevents such a condition from naturally taking place. Numerous means have been devised to overcome this problem; high-quality-factor resonant cavities [1], quasi-phase matching (QPM) [2], form birefringence [3], and photonic bandgap structures [4] were all studied. While these solutions produce routes to phase matching, they provide devices that are difficult to integrate with other active and passive photonic components. One approach, which uses QPM, lends itself to monolithic integration [5]. Thus far, it has been associated with excess optical losses and low effective nonlinearity. Another promising demonstration of QPM in semiconductors relies on inverting the domain of the nonlinearity by growing GaAs/AlGaAs semiconductors with different orientations [2]. Operational table-top OPOs were nonetheless demonstrated using these materials [6]. Monolithic integration is likely to prove challenging, as the crystalline regrowth will be obstructed by the rapid oxidation rate of AlGaAs. Judging by the progress reported using the techniques discussed above; a means of phase matching that is readily integrable with mainstream photonic devices using available technologies is yet to be found.

Recently we have reported a novel approach to phase matching [7]. The technique exploits the modal dispersion properties of Bragg reflection waveguides (BRWs) [8] in comparison with those of conventional total internal reflection waveguides to match the modal index of the interacting waves. The technique was studied for SHG at a fundamental of 1550 nm [9]. Several advantages characterize this technique over its counterparts. These include its monolithic structure, the lack of material structuring or modulation along the direction of wave propagation, and its ability to provide control over the interacting waves' dispersion properties. In this Letter, we present measurements of SHG for a pump at 1587.8 nm generating second harmonic (SH) at 794 nm using this technique.

The structure was nominally undoped and grown using metal-organic chemical vapor deposition (MOCVD). It had a 500 nm GaAs buffer grown on the GaAs substrate first. The lower cladding consisted of 10 periods of a Bragg stack with 278 nm of $Al_{0.6}Ga_{0.4}As$ and 118 nm of $Al_{0.2}Ga_{0.8}As$. The waveguide core was made out of $Al_{0.4}Ga_{0.6}As$ and had a thickness of 328 nm. The top cladding was composed of 8 periods of the same Bragg stack as the lower cladding. The structure was capped with 50 nm of GaAs. Using the $Al_xGa_{1-x}As$ refractive index data from Adachi [10], the structure provides an effective index for the TE-polarized fundamental mode at 1.55 μm equal to that of the TM-polarized SH at 775 nm [7]. This arrangement is consistent with the polarization conditions for type I phase matching of the bulk $\chi^{(2)}_{xyz}$ (d_{14}) coefficient [9]. The calculated field

0146-9592/07/162399-3/$15.00

intensity of both the SH and fundamental for this waveguide are shown in Fig. 1.

The characterization was carried out using a singly-resonant KTP OPO synchronously pumped by a mode-locked Ti:sapphire laser. Output pulses with full width at half-maximum (FWHM) durations between 1.5 and 2.5 ps, a 75.6 MHz repetition rate and a maximum average power of ~176 mW were obtained at the input facet of the sample. Pulses with a center wavelength around 1550 nm were end-fire coupled into a 2.38 mm long sample using an antireflection-coated 40× objective lens. A cylindrical lens with a focal length of 150 mm was used at the input to render the beam elliptical. This enhances the coupling efficiency into the slab and maintains a minimum beam waist inside the sample. After the light was coupled into the slab with the aid of an infrared camera, the output of the slab was focused onto a powermeter to measure the amount of transmission through the samples. The light was then coupled into an optical spectrum analyzer to track changes in the output spectrum. Through modeling the incident beam, it was predicted that the optimum configuration obtained using this setup provides a beam with a spot size of 37.5 μm at the sample facet. The beam focuses in the horizontal direction 1 mm inside the sample with a minimum beam waist of 27.8 μm. At the output of the sample the beam spot size is 50 μm. The beam waist remains constant in the vertical direction thanks to the vertical guiding structure as can be seen in Fig. 1. The coupling efficiency into the slab was measured using samples with different lengths to be ~20% ±5%. The propagation loss of the sample was found to be ~2.5 cm^{-1} ± 1.5 cm^{-1}. Using the BRW in a slab arrangement rather than in a ridge waveguide arrangement has been chosen as a first step to test these structures. This helps in the study of the properties of the phase-matching technique while eliminating any tolerances induced by the two-dimensional ridge fabrication. In ridge waveguide configuration, these tolerances would be convoluted with those introduced during molecular beam epitaxy growth, which will impede the ability to analyze the inherent properties of the phase-matching technique.

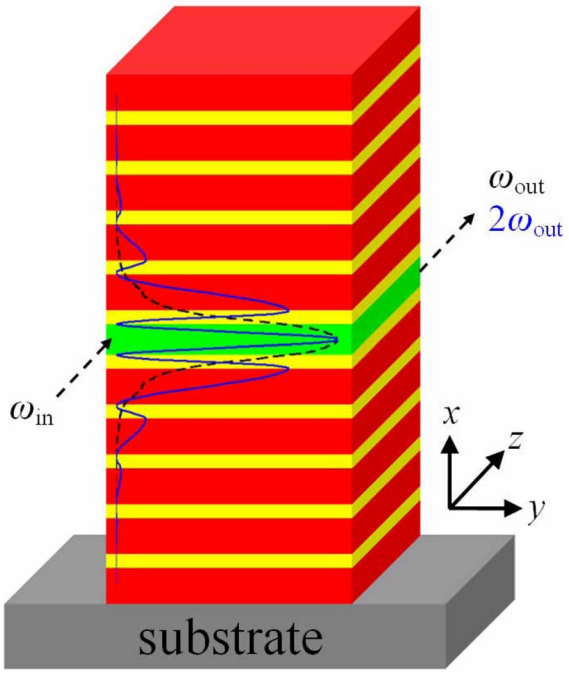

Fig. 1. (Color online) Intensity of the total internal reflection mode at 1550 nm and the Bragg reflection mode at 775 nm in the Bragg reflection waveguide studied. Both are superimposed on a schematic of the structure. The dashed line is for the fundamental, while the solid line is for the SH.

Initially, the power-in/power-out relation has been inspected to ensure that no dominant two-photon absorption effects take place. Its effects were eliminated by design since the operating wavelengths are at more than 173 meV below the half-bandgap of the lowest Al-containing layers in the structure ($Al_{0.2}Ga_{0.8}As$). The TM-polarized SH output power is shown in Fig. 2 for different TE-polarized pump wavelengths. No SH power could be detected when the input is switched to TM polarization. As can be seen in Fig. 2, un-phase-matched SH power could be detected throughout the range of wavelengths studied. However, at the regime where the BRW phase matching takes place (at λ_{pump} = 1587.8 nm) the SH output power increases by one order of magnitude. This phase-matching feature exhibited a FWHM of 2.22 nm. The quadratic dependence of the SH power on the pump power is confirmed on- and off-resonance as shown in Fig. 3. The slope of both curves is approximately equal to 2 on a log–log scale, confirming the parabolic power dependence. No sign of saturation could be detected.

Further insight can be acquired when the spectra of the SH are inspected. Spectra for two TE-polarized pump signals with wavelengths of 1578.8 and 1587.8 nm are shown in Fig. 4. They are denoted Fn1 and Fn2, respectively. Also plotted are the spectra of their corresponding TM-polarized SH signals at 789.5 and 794 nm, which are denoted SH1 and SH2,

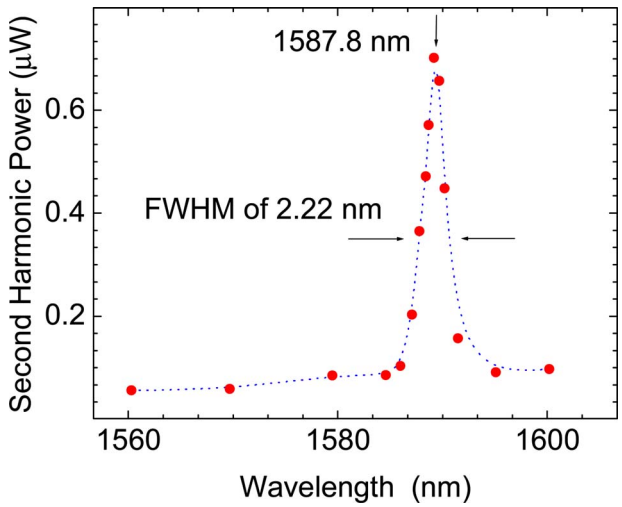

Fig. 2. (Color online) SH power inside the sample by the output facet as a function of the pump wavelength for an input power of 15.3 mW inside the sample by the input facet.

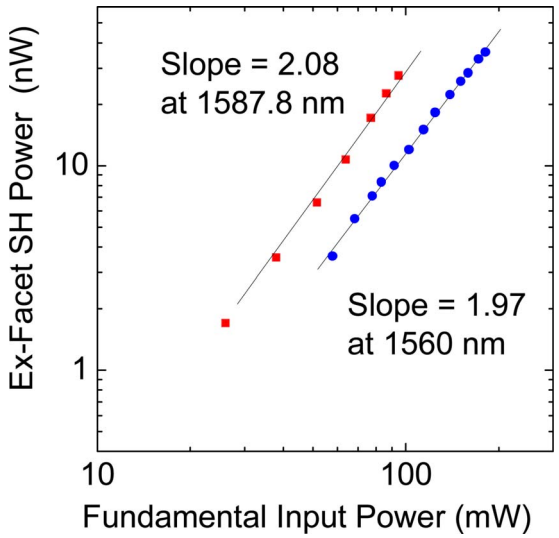

Fig. 3. (Color online) Dependence of the SH power on that of the pump for two wavelengths, 1560 and 1587.8 nm.

respectively. The spectral width of the un-phase-matched signal SH1 (FWHM, 1.21 nm) is close to half of that of the pump wavelength (FWHM, 2.88 nm). This is not the case for SH2, where phase matching takes place. In this case, the SH spectral width (FWHM, 0.43 nm) is nearly one order of magnitude smaller than the FWHM of its corresponding pump (FWHM, 3.54 nm). This is strong evidence of the change in the nature of SH and its transition from un-phase-matched into phase matched at the wavelength of 1587.8 nm. The narrower spectral width suggests that the limitation of the phase-matching bandwidth is determined by the BRW structure. From previous work [9], we were able to predict the bandwidth measured for these structures. Given the numbers presented above the SH conversion efficiency is of the order of 0.001%. It must be emphasized that there is ample room for this number to dramatically increase. First, two-dimensional waveguides will provide at least one order of magnitude increase in the pump intensity. Second, using two-dimensional waveguides will enable using longer

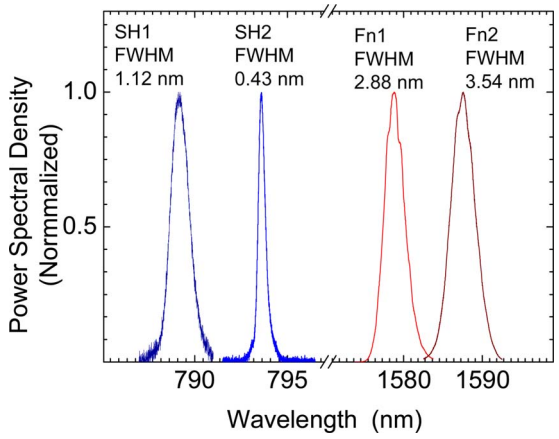

Fig. 4. (Color online) Spectra of the input pump at two wavelengths (Fn1, 1578.8 nm and Fn2, 1587.8 nm) and the spectra of the corresponding SH signals (SH1, 789.5 nm and SH2, 794 nm).

samples, which will in turn enhance the overall performance particularly given the low propagation losses offered by this technique. Third, the BRW design offers the possibility of tuning the group velocity mismatch between the interacting waves, which should further enhance the efficiency. Fourth, the laser pulses used exhibited a bandwidth larger than that of the phase-matching technique used. Using a pulsed source with pulses of a few hundred picoseconds and hence a narrower bandwidth could enhance the portion of the pump power utilized in the SHG process.

It should be noted the samples were designed for phase matching at 775 nm. However, variation of the core thickness or Al composition from design during growth can explain this wavelength mismatch. Metal-organic chemical vapor deposition growth tolerances are likely to be present in the cladding and core layers. The mismatch observed requires a change in the core thickness of ±8 nm or change in the core Al concentration of ±4 % [7,9]. Due to the nature of waveguiding in BRWs, tuning the phase-matching wavelength cannot be achieved via simple temperature tuning. Instead, tuning could take place via selectively influencing the refractive index of the core layer using current injection or electro-optic effects in p-i-n structures [7,9].

In summary, we presented what is to our knowledge the first observation of second-harmonic generation by type I phase matching in Bragg reflection waveguides. SH power of 0.7 μW was observed for an average pump power of 25.2 mW and a pulse width of ~2 ps at a repetition rate of 75.6 MHz. The bandwidth of the SH was found to be equal to 0.43 nm, agreeing with the theoretical predictions.

The authors are grateful to Joachim Meier for valuable technical assistance and for the assistance of J. S. Aitchison, R. J. D. Miller, and M. Cowan. The authors gratefully acknowledge the support of NSERC Discovery Grant number 293258/5 and CMC Microsystems.

References

1. R. Haidar, N. Forget, and E. Rosencher, IEEE J. Quantum Electron. **39**, 569 (2003).
2. C. B. Ebert, L. A. Eyres, M. M. Fejer, and J. H. Harris, J. Cryst. Growth **227**, 183 (1999).
3. A. Fiore, S. Janz, L. Delobel, P. van der Meer, P. Bravetti, V. Berger, and E. Rosencher, Appl. Phys. Lett. **72**, 2942 (1998).
4. D. Faccio, F. Bragheri, and M. Cherchi, J. Opt. Soc. Am. B **21**, 296 (2004).
5. A. S. Helmy, D. C. Hutchings, T. C. Kleckner, J. H. Marsh, A. C. Bryce, J. M. Arnold, C. R. Stanley, J. S. Aitchison, C. T. A. Brown, K. Moutzouris, and M. Ebrahimzadeh, Opt. Lett. **25**, 1370 (2000).
6. K. L. Vodopyanov, O. Levi, P. S. Kuo, T. J. Pinguet, J. S. Harris, M. M. Fejer, B. Gerard, L. Becouarn, and E. Lallier, Opt. Lett. **29**, 1912 (2004).
7. A. S. Helmy, Opt. Express **14**, 1243 (2006).
8. P. Yeh and A. Yariv, Opt. Commun. **19**, 427 (1976).
9. B. R. West and A. S. Helmy, IEEE J. Sel. Top. Quantum Electron. **12**, 431 (2006).
10. S. Adachi, J. Appl. Phys. **58**, R1 (1985).